Dynamics of a Tunable Superfluid Junction

L. J. LeBlanc, A. B. Bardon, J. McKeever, M. H. T. Extavour, D. Jervis, and J. H. Thywissen
Department of Physics, University of Toronto, 60 St. George, Toronto ON, Canada, M5S 1A7

F. Piazza and A. Smerzi
INO-CNR, BEC Center, and Dipartimento di Fisica, Via Sommarive 14, 38123 Povo, Trento, Italy
(Received 17 June 2010; published 12 January 2011)

We study the population dynamics of a Bose-Einstein condensate in a double-well potential throughout the crossover from Josephson dynamics to hydrodynamics. At barriers higher than the chemical potential, we observe slow oscillations well described by a Josephson model. In the limit of low barriers, the fundamental frequency agrees with a simple hydrodynamic model, but we also observe a second, higher frequency. A full numerical simulation of the Gross-Pitaevskii equation giving the frequencies and amplitudes of the observed modes between these two limits is compared to the data and is used to understand the origin of the higher mode. Implications for trapped matter-wave interferometers are discussed.

DOI: 10.1103/PhysRevLett.106.025302 PACS numbers: 67.85.−d, 03.75.Lm, 67.10.Jn, 74.50.+r

Quantum mechanical transport is a consequence of spatial variations in phase. Superfluids behave like perfect inviscid irrotational fluids, whose velocity is the gradient of a local phase, so long as the confining potential is smooth on the scale of the healing length. Where the density is small, as it is near surfaces, quantum kinetic terms must be added to the classical hydrodynamic equations. Macroscopic quantum coherence phenomena, such as Josephson effects, emerge when superfluids are weakly linked across such a barrier region.

Josephson effects have been demonstrated with superconductors [1], liquid helium [2,3], and ultracold gases in both double-well [4,5] and multiple-well optical trapping potentials [6]. The canonical description of these experiments employs a two-mode model [7–9], in which a sinusoidal current-phase relationship emerges. Hydrodynamics has also been studied in both liquids and ultracold gases [10]. The relative diluteness of gases makes a satisfying *ab initio* description possible [11].

In this Letter, we study the transport of a Bose-Einstein condensate (BEC) between two wells separated by a tunable barrier and observe the crossover from hydrodynamic to Josephson transport. As the barrier height V_b is adjusted from below to above the BEC chemical potential, μ, the density in the link region decreases until it classically vanishes when $V_b = \mu$. The healing length in the link region, ξ, increases with V_b and dictates the nature of transport through this region. Oscillatory dynamics spanning three octaves are observed as we smoothly tune ξ from $0.3d$ to $2d$, where d is the separation between the wells.

Examination of the dynamics of an elongated BEC in a double well is timely. Recent experiments have created squeezed and entangled states by adiabatically splitting a BEC [12–14]. The degree of squeezing inferred in the elongated case [12,13] seems to exceed what would be expected in thermal equilibrium [14], raising the possibility that out-of-equilibrium dynamics may be important. With much remaining to be explored in these systems, this work represents the first study of the dynamics in the crossover regime.

Our experiment begins as ^{87}Rb atoms in the $|F = 2, m_F = 2\rangle$ ground state are trapped on an atom chip and evaporatively cooled in a static magnetic potential $\mathbf{B}_S(\mathbf{r})$, as described elsewhere [15]. To prevent gravitational sag and to compress the trap in the weak direction (with characteristic trap frequency $\omega_y = 2\pi \times 95$ Hz), we add an attractive optical potential with a 1064 nm beam. We dress the static potential with an oscillating radio-frequency (rf) magnetic field [16,17] radiating from two parallel wires on the atom chip [Fig. 1(a)]. In the rotating-wave approximation, the adiabatic potential created by the combination of the static chip trap, the rf dressing, and the optical force is

$$U(\mathbf{r}) = m'_F \mathrm{sgn}(g_F)\hbar\sqrt{\delta(\mathbf{r})^2 + \Omega_\perp^2(\mathbf{r})} + \tfrac{1}{2}m\omega_y^2 y^2, \quad (1)$$

where $m'_F = 2$ is the effective magnetic quantum number, $\delta(\mathbf{r}) = \omega_{\mathrm{rf}} - |\mu_b g_F B_S(\mathbf{r})/\hbar|$ is the detuning, $\Omega_\perp(\mathbf{r}) = |\mu_b g_F B_{\mathrm{rf},\perp}(\mathbf{r})/2\hbar|$ is the rf Rabi frequency, $B_{\mathrm{rf},\perp}(\mathbf{r}) = |\mathbf{B}_S(\mathbf{r}) \times \mathbf{B}_{\mathrm{rf}}(\mathbf{r})|/|\mathbf{B}_S(\mathbf{r})|$ is the amplitude of the rf field locally perpendicular to $\mathbf{B}_S(\mathbf{r})$, μ_b is the Bohr magneton, g_F is the Landé g factor, $\hbar$ is the reduced Planck's constant, and m is the atomic mass. By assuming the individual wells are harmonic near each minimum, calculations show that $\omega_z = 2\pi \times 425$ Hz, and ω_x varies from $2\pi \times 350$ Hz to $2\pi \times 770$ Hz as we tune from low to high barriers. For comparison between theory and experiment, we account for small corrections to Eq. (1) beyond the rotating-wave approximation [18,19].

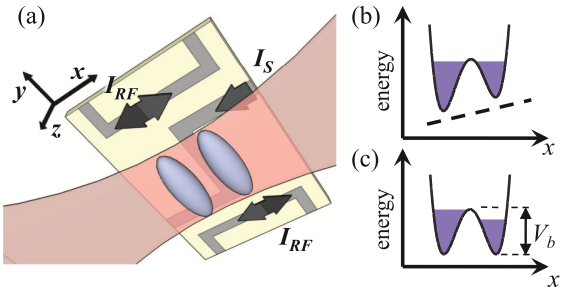

FIG. 1 (color online). (a) Schematic of atom chip double-well trap. Central Z wire [34] carries static trapping current, $I_S = 2$ A, which, with uniform external fields $\mathbf{B}_{\text{ext}} = \langle 2.2, 0.11, 0\rangle$ mT, results in an Ioffe-Pritchard style trap with harmonic trapping frequencies $(\omega_{x_0,z_0}, \omega_{y_0}) = 2\pi \times (1300, 10)$ Hz. Side wires are 1.58 mm from trap center and carry rf currents with amplitude I_{rf}. This rf current produces a z-polarized field at the trap location with amplitude $B_{\text{rf}} = 23.6 \pm 0.6$ μT [peak Rabi frequency $\Omega = 2\pi \times (82 \pm 2\,\text{kHz})$]. A levitation beam [gray (pink)] is positioned to provide a force-canceling gravity (z direction) while compressing the sample along y. Atoms are trapped 190 μm from the chip surface. (b) A schematic one-dimensional cut at $t = -0.5$ ms through trapping potential along x (solid line) in the presence of linear bias (dashed line) and (c) balanced potential at $t = 0$, with $\mathcal{Z}_0 \neq 0$.

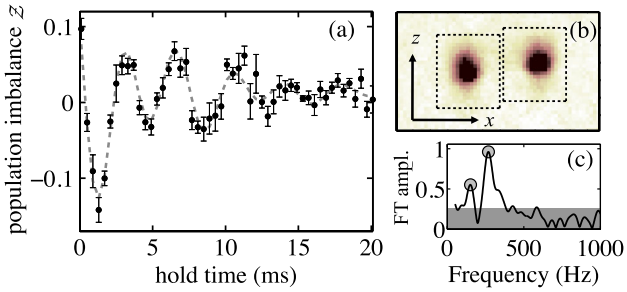

FIG. 2 (color online). (a) Population imbalance, $\mathcal{Z}$, vs time for $\delta = 2\pi \times (0.1 \pm 0.5)$ kHz, $N = 5900 \pm 150$. The dashed line is a decaying two-frequency sinusoidal fit to the data, using two fixed frequencies from the FT (lower inset). Each point is the average of six repetitions of the experiment; error bars are statistical. (b) Averaged absorption image after separation and 1.3 ms time of flight, with right and left measurement regions (dashed boxes) indicated. (c) FT amplitude spectrum of data showing two distinct peaks at 268 ± 6 and 151 ± 13 Hz rising above the noise floor (grey).

After turning on the dressing field at a frequency $\omega_{\text{rf}} = 2\pi \times 765$ kHz, where the trap is a single well, we evaporatively cool to produce a BEC with no discernible thermal fraction. In 20 ms, we adiabatically increase ω_{rf} to a new value characterized by $\delta_0 \equiv \delta(\mathbf{r} = \mathbf{0})$, such that the barrier V_b rises and the dressed state potential splits along the x direction into two elongated traps [20].

Using a second 1064 nm beam weakly focused off-center in x, an approximately linear potential is added across the double-well junction to bias the population towards one well [Fig. 1(b)]. By applying the bias beam before and during the splitting process, we prepare systems of atoms with a population imbalance $\mathcal{Z} \equiv (N_R - N_L)/(N_R + N_L)$, where N_R (N_L) is the number of atoms in the right (left) well. The range of initial population imbalances $\mathcal{Z}_0 = \mathcal{Z}(t = 0)$ we use is 0.05 to 0.10, small enough to avoid self-trapping [4]. To initiate the dynamics, the power of the bias beam is ramped off in 0.5 ms (faster than the population dynamics) and the out-of-equilibrium system is allowed to evolve for a variable time t in the symmetric double well [Fig. 1(c)].

To measure the time-dependent population $\mathcal{Z}(t)$, we freeze dynamics by rapidly increasing both B_{rf} and ω_{rf} to separate the wells by 70 μm, where $V_b/\mu \sim 10^4$. We release the clouds from the trap and perform standard absorption imaging along y after 1.3 ms time-of-flight [Fig. 2(b)]. Analysis of these images allows us to determine N_R and N_L to a precision of ± 50 atoms.

Upon release of the potential bias, we find that the population $\mathcal{Z}(t)$ oscillates about $\mathcal{Z} = 0$ [Fig. 2(a)] [21]. To analyze the dynamics, we use a Fourier transform (FT) to find the dominant frequency components [Fig. 2(c)]. We repeat this measurement at many values of V_b/μ, where μ is the Thomas-Fermi chemical potential, by varying δ_0. For the purposes of this analysis, we ignore the decay of this signal, the $1/e$ time constant of which is typically two oscillation periods.

When the barrier is low, $\mathcal{Z}(t)$ consistently displays two dominant frequency components. For higher barriers, the amplitude of the higher-frequency mode decreases until only a single frequency rises above the noise floor. The white points in Fig. 3 give these frequencies as a function of the experimental parameter δ_0 and the calculated ratio of barrier height to chemical potential, V_b/μ. The ensembles used in Fig. 3 had total atom number $N = 6600 \pm 400(\pm 1700)$, where the error bar is statistical (systematic).

In the low- and high-barrier limits, simple models can be used to understand the dynamics. For low barriers, the hydrodynamic equations of motion can be used to estimate the frequency of population oscillation. Assuming a harmonic population response for some $\mathcal{Z}_0$, the response frequency is

$$\omega_{\text{HD}}^2 = -\frac{2}{mN\mathcal{Z}_0}\int_S \rho\hat{n}\cdot\vec{\nabla}(U + g\rho)dS, \qquad (2)$$

where ρ is the density of the condensate at $t = 0$, S is the surface in the y-z plane bisecting the double well, and $\hat{n}$ is the vector normal to this surface. Plotting ω_{HD} in Fig. 3 (dotted line), we find good agreement with the lower frequency mode at low barriers. Since tunneling cannot contribute to hydrodynamic transport, $\omega_{\text{HD}} \to 0$ as $V_b \to \mu$. The breakdown in hydrodynamics also coincides with an increasing healing length, as shown in the inset of Fig. 3.

In the opposite limit, when tunneling dominates transport, a Josephson model [8] accurately predicts the frequency of the highest barrier points,

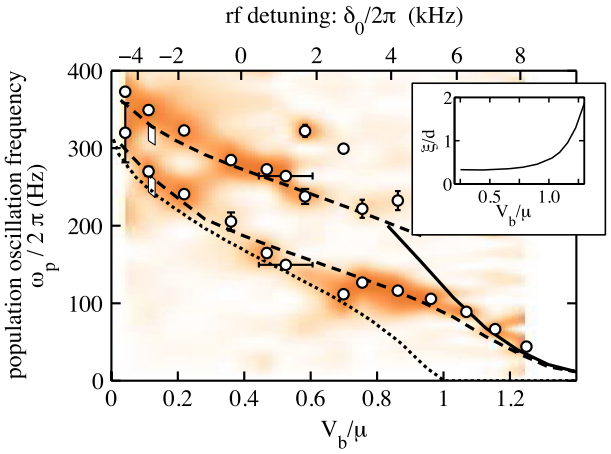

FIG. 3 (color online). Frequency components of population imbalance vs rf detuning (measured) and barrier height to chemical potential ratio (calculated). Experimental points (white circles) represent the two dominant Fourier components at each detuning; error bars represent uncertainty contributed by noise in the FT from a single time series, but do not include shot-to-shot fluctuations. The spectral weight is represented through the color map, which has been linearly smoothed between discrete values of V_b/μ and darker colors indicate greater spectral weight. All calculations use $N = 8000$ and $Z_0 = 0.075$, and a single-parameter fit of the data to the GPE curves shifts all experimental points by $\delta_{\text{shift}} = 2\pi \times 5.1$ kHz [19] to compensate for a systematic unknown in $B_S(\mathbf{0})$. Statistical vertical error bars are shown, while a typical horizontal statistical error bar is shown at $V_b/\mu \approx 0.5$. Dashed lines represent 3D GPE frequencies, the solid line the plasma oscillation frequency predicted by the Josephson model, ω_p, and the dotted line the hydrodynamic approximation, $\omega_{\text{HD}}/2\pi$. White bars at $V_b/\mu \sim 0.1$ indicate the bounds of the GPE simulation corresponding to the systematic plus statistical uncertainty in atom number. Inset: ratio of healing length, ξ, to interwell distance, d, as a function of V_b/μ. ξ is calculated at the center of the barrier.

$$\omega_p^2 = \frac{1}{\hbar^2}\Delta E\left(\Delta E + N\frac{\partial \mu_{\text{loc}}}{\partial N}\right), \tag{3}$$

where ΔE is the energy difference between the symmetric and antisymmetric ground states of the double-well potential, N is total atom number, and μ_{loc} is the chemical potential on one side of the well [19]. The agreement is surprisingly good even for V_b just above μ, beyond which the frequency decreases exponentially. To our knowledge, this constitutes the first direct observation of tunneling transport of neutral atoms through a magnetic barrier, only inferred, for instance, in Refs. [12,22].

To explain the crossover behavior and the existence of the higher-frequency mode, we turn to numerical solutions of a time-dependent three-dimensional Gross-Pitaevskii equation (GPE) [8,23], which should describe all mean-field dynamics at $T = 0$. The slope and separation of the measured frequencies are well captured by the GPE, as shown in Fig. 3, though the decay of population imbalance is not reproduced by these simulations.

The structure and origin of the higher-lying dynamical mode can be studied within the simulations. If our trap were smoothly deformed to a spherical harmonic potential, the two observed modes would connect to odd-parity modes [11]: the lower mode connects to the lowest $m = 0$ mode (coming from the $\ell = 1$ mode at spherical symmetry, where the quantum numbers ℓ and m label the angular momentum of the excitation and its projection along the axis of symmetry, y, respectively), while the higher mode originates from the lowest $m = 2$ mode ($\ell = 3$ at spherical symmetry) [24].

With insight from GPE simulations, the observation of a second dynamical mode, which was not seen in previous experimental work [4,5], can be explained. In a purely harmonic trap, a linear bias excites only a dipole mode [25]. By breaking harmonicity along the splitting direction, x, the barrier allows the linear perturbation ($\ell = 1$, $m = 0$, where x is the azimuthal axis) to excite multiple Bogoliubov modes [26]. Numerical studies show that two additional ingredients are required to excite the higher mode. First, atom-atom interactions couple the x excitation to the transverse (y, z) motion through the nonlinear term in the GPE. Second, the anisotropy of the trap in the y-z plane mixes the $m = 0$ and $m = 2$ modes such that each of the resulting modes drives population transfer between wells.

Figure 4 shows the relative strength $R_1 = a_1/(a_1 + a_2)$ of the lower frequency mode as a function of the barrier height. The amplitude a_1 (a_2) of the lower (higher) frequency mode is extracted from a decaying two-frequency sinusoidal fit. The modes have comparable strength, even in the linear perturbation regime, when the barrier is below the chemical potential. The small spread in the GPE amplitudes shown by the grey band indicates that the higher mode is excited independently of the initial imbalance, and is not simply due to a high-amplitude nonlinearity.

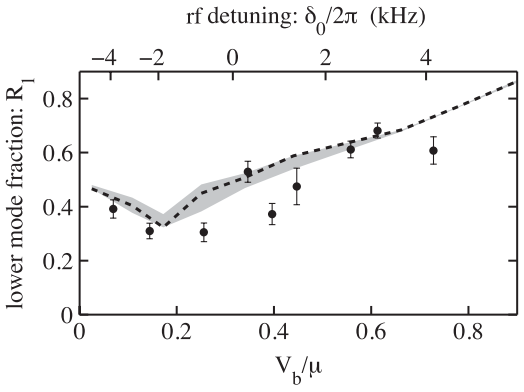

FIG. 4. Fraction of low-frequency mode in population dynamics. Dashed line shows the GPE simulation for 8000 atoms with initial imbalance $Z(0) = 0.075$. The grey shaded area represents the variation of the GPE calculations over the range of $Z(0) = 0.05$ to 0.10. The vertical error bars are statistical; the statistical uncertainty in δ is $2\pi \times 0.5$ kHz (not shown). The GPE calculation gives $R_1 = 1$ when $V_b/\mu \simeq 1.1$.

The trend in R_1 reflects the shape of the trap. When the barrier is raised from zero, the higher mode is at first more easily excited due to an increased anharmonicity along x as the trap bottom becomes flatter. By further increasing the barrier, the higher-frequency mode disappears from the population oscillation spectrum due to the vanishing excitation of transverse modes. As the wave functions in each individual well are increasingly localized to the effectively harmonic minima, the linear bias no longer excites intrawell transverse motion. Furthermore, in the linear perturbation regime, the interwell Josephson plasma oscillation, like all Bogoliubov modes, cannot itself trigger any other collective mode.

In conclusion, we have studied the quantum transport of a BEC in a double-well potential throughout the crossover from hydrodynamic to Josephson regimes. Apart from fundamental interest, knowing and controlling the nature of superfluid transport is crucial for technological applications of weak-link-based devices, such as double-slit interferometers [12,20,27–29]. The adiabatic transformation of a BEC from a single- to a double-well trapping potential has been discussed in recent experimental works [12,14,22,30,31] in the context of the Josephson model, valid at high barriers [32]. Our work demonstrates that for $V_b < \mu$, the lowest mode frequency will lie below that estimated by the Josephson model. Furthermore, the higher-lying mode we observe approaches the lowest collective mode as $\omega_y \ll \omega_z$ [19] and may be important to the dynamics of splitting in strongly anisotropic double wells [12,33]. Whether using splitting to prepare entangled states [14], or recombination [31] to perform closed-loop interferometry [30], an improved understanding of double-well dynamics provides a foundation for controlling mesoscopic superfluids.

We would like to thank T. Schumm for early experimental work, A. Griffin, P. Krüger, D. McKay, M. Sprague, and E. Zaremba for helpful discussions, and J. Chwedeńczuk for help with numerical simulations of the GPE. This work has been generously supported by CIfAR, CFI, CQIQC, and NSERC.

[1] P. W. Anderson and J. M. Rowell, Phys. Rev. Lett. **10**, 230 (1963).
[2] S. Pereverzev, A. Loshak, S. Backhaus, J. Davis, and R. Packard, Nature (London) **388**, 449 (1997).
[3] S. Backhaus, S. Pereverzev, A. Loshak, J. Davis, and R. Packard, Science **278**, 1435 (1997).
[4] M. Albiez *et al.*, Phys. Rev. Lett. **95**, 010402 (2005).
[5] S. Levy, E. Lahoud, I. Shomroni, and J. Steinhauer, Nature (London) **449**, 579 (2007).
[6] F. S. Cataliotti *et al.*, Science **293**, 843 (2001); O. Morsch and M. Oberthaler, Rev. Mod. Phys. **78**, 179 (2006); See also B. P. Anderson and M. A. Kasevich, Science **282**, 1686 (1998).
[7] B. D. Josephson, Phys. Lett. **1**, 251 (1962).
[8] A. Smerzi, S. Fantoni, S. Giovanazzi, and S. R. Shenoy, Phys. Rev. Lett. **79**, 4950 (1997); I. Zapata, F. Sols, and A. J. Leggett, Phys. Rev. A **57**, R28 (1998); S. Raghavan, A. Smerzi, S. Fantoni, and S. R. Shenoy, Phys. Rev. A **59**, 620 (1999); D. Ananikian and T. Bergeman, Phys. Rev. A **73**, 013604 (2006).
[9] A. Smerzi and A. Trombettoni, Phys. Rev. A **68**, 023613 (2003).
[10] D. S. Jin, J. R. Ensher, M. R. Matthews, C. E. Wieman, and E. A. Cornell, Phys. Rev. Lett. **77**, 420 (1996); K. M. O'Hara *et al.*, Science **298**, 2179 (2002); T. Bourdel *et al.*, Phys. Rev. Lett. **93**, 050401 (2004).
[11] S. Stringari, Phys. Rev. Lett. **77**, 2360 (1996); D. A. W. Hutchinson and E. Zaremba, Phys. Rev. A **57**, 1280 (1998).
[12] G.-B. Jo *et al.*, Phys. Rev. Lett. **98**, 030407 (2007).
[13] G.-B. Jo *et al.*, Phys. Rev. Lett. **99**, 240406 (2007).
[14] J. Esteve, C. Gross, A. Weller, S. Giovanazzi, and M. K. Oberthaler, Nature (London) **455**, 1216 (2008).
[15] S. Aubin *et al.*, Nature Phys. **2**, 384 (2006).
[16] Y. Colombe *et al.*, Europhys. Lett. **67**, 593 (2004).
[17] I. Lesanovsky *et al.*, Phys. Rev. A **73**, 033619 (2006).
[18] S. Hofferberth, B. Fischer, T. Schumm, J. Schmiedmayer, and I. Lesanovsky, Phys. Rev. A **76**, 013401 (2007).
[19] See supplementary material at http://link.aps.org/supplemental/10.1103/PhysRevLett.106.025302.
[20] T. Schumm *et al.*, Nature Phys. **1**, 57 (2005).
[21] When the average value of $\mathcal{Z}$ differs from zero, we subtract the average $\overline{\mathcal{Z}}$ from all values of $\mathcal{Z}(t)$. In all experiments, $|\overline{\mathcal{Z}}| < 0.05$.
[22] K. Maussang *et al.*, Phys. Rev. Lett. **105**, 080403 (2010).
[23] L. P. Pitaevskii, Sov. Phys. JETP **13**, 451 (1961); E. P. Gross, Nuovo Cimento **20**, 454 (1961); J. Math. Phys. (N.Y.) **4**, 195 (1963).
[24] We checked this numerically by deforming our trap into a fully harmonic axially symmetric trap, and following the mode frequencies throughout this process.
[25] W. Kohn, Phys. Rev. **123**, 1242 (1961).
[26] H. Ott *et al.*, Phys. Rev. Lett. **91**, 040402 (2003).
[27] Y. Shin *et al.*, Phys. Rev. Lett. **95**, 170402 (2005).
[28] C. Gross, T. Zibold, E. Nicklas, J. Estéve, and M. K. Oberthaler, Nature (London) **464**, 1165 (2010).
[29] F. Baumgartner *et al.*, Phys. Rev. Lett. **105**, 243003 (2010).
[30] Y.-J. Wang *et al.*, Phys. Rev. Lett. **94**, 090405 (2005).
[31] G.-B. Jo *et al.*, Phys. Rev. Lett. **98**, 180401 (2007).
[32] A. J. Leggett and F. Sols, Phys. Rev. Lett. **81**, 1344 (1998).
[33] A. Polkovnikov and V. Gritsev, Nature Phys. **4**, 477 (2008).
[34] J. Reichel, Appl. Phys. B **74**, 469 (2002).